Egyptian Journal of Chemistry
http://ejchem.journals.ekb.eg/

Synthesis Of Linbo3 Microstructures: Structural, Optical And, Surface Morphologyu Sing Chemical Bath Deposition (Cbd) Method with Out Post Heat Treatment.

Rawan Bashar Fadhil [a] Evan T. Salim [a*] Wafaa. K. Khalef [a]
[a] *Applied science department, University of Technology-Iraq, 10066 Baghdad, Iraq*

Abstract.
A cost-effective, low-temperature, chemical bath deposition technique has been widely used in preparing Lithium-niobate (LiNbO3) nanostructures. The deposition process was maintained over a quartz substrate for two different samples, with and without annealing at 500 °C. A hexagonal structured $LiNbO_3$ with maximum diffraction peak at (012) diffraction plane for both samples and with a slight shifting toward $2\theta = 23.86$ for the sample without the post-heat treatment. After the annealing process, the optical absorption reveals the lower absorbance of the annealed sample with the energy gap shifting from 3.64 to 3.65. The FTIR results ensure the formation of the $LINBO_3$ material and agree with X-ray diffraction (XRD) results.
Keywords: Lithium niobate; CBD methods; structural properties; optical properties; morphological properties

Introduction

The LiNbO3 is a significant optical material that was broadly used in the Photonics industries because of its excellent acoustic-optical, piezoelectric, pyroelectrical, electro-optics and photo-refractive properties; owing to its large second-order nonlinearities, it is one of the most effective materials for electro-optic application [1–6]. The LiNbO3 is used to manufacture optical waveguides, nonlinear optics for telecommunication [7–11], photonic fiber crystal and electro-optic modulation [12–14]. It found be successfully integrated in optoelectronic devices and components from fiber-based communication to wireless communication and Micro-Electro-Mechanical Systems (MEMS) [17]. Among the most optical applications are filters and modulators with laser source on a single $LiNbO_3$ wafer, particularly promising in optical channel waveguides and integrated optics. In the last few years, LN has attracted much researchers' interest because of its high-quality, low-optical-loss source material for waveguide applications; for example, $LiNbO_3$ on insulator (LNOI) is performing a substantive role in photonic integrated circuits [18], solid-state tuning behaviour [19], and Tunable filter with broadband applications [20]. The versatile applications require multi forms of $LiNbO_3$, for instance, bulk as Mach-Zehnder modulator [21], composites [22], and thin-film forms [23], which are possible to use in physical structures like waveguides [24][25]. Owing to its importance in a wide range of applications $LiNbO_3$ was studied over many decades. Various methods have been utilised to synthesise $LiNbO_3$ nanocrystals, such as soft-chemistry, sol-gel [26–28], pulsed laser deposition (PLD) and pulse laser ablation (PLA) [29, 30], metal-organic chemical vapour deposition (MOCVD) [31], liquid phase epitaxial (LPE) [32], magnetron sputtering [33] and chemical hydrothermal technique [34, 35]. $LiNbO_3$ nanostructures were prepared successfully at low temperatures in several works[15]. The complete protocol showed by Grigas, A. et.al.[16], implies a Li H-induced reduction of NbCl5 followed by in situ spontaneous oxidation into low-valence niobium nano-oxides. Subsequently, these niobium oxides are exposed to air atmosphere thereby achieving pure Nb_2O_5. Finally, the stable Nb_2O_5 is converted into $LiNbO_3$ nanoparticles during the controlled hydrolysis of the LiH excess [16]. In other work the $LiNbO_3$ spherical nanoparticles with a diameter of approximately 10 nm was also prepared by impregnating a meso-porous silica matrix with a mixture of a combined aqueous solution of $LiNO_3$ and $NH_4NbO(C_2O4)_2$ then followed by heating in an infrared furnace for 10 min. other previous preparation processes include a

*Corresponding author e-mail: Tel. + (964) 7715752087, E-mail: 100354@uotechnology.edu.iq
Receive Date: 29 March 2022, **evise Date:** 02 July 2022, **Accept Date:** 30 July 2022, **First Publish Date:** 30 July 2022
DOI: 10.21608/EJCHEM.2022.129669.5749

post-heat treatment step. In 2013, D. A. Kiselev et al, synthesised the LiNbO3 films using Rf magnetron sputtering while they investigated the effects of annealing on the structure of the thin films at varying temperatures of 550 °C, 700 °C and 1000 °C. The results demonstrate that two $LiNbO_3$ phases are formed as a result of post-growth annealing [36]. Later in 2017, Makram A. Fakhri et al., prepared a high-purity $LiNbO_3$ Nano and Micro-structure by depositing it on a quartz substrate at three different annealing temperatures. The measurements showed that as the annealing temperature increased, the structure was crystalline-like and the grains are regularly distributed within the film [37]. Other related work done in 2019 by Viktor S. Klimin et al., also included the effect of annealing on the physical properties of the $LiNbO_3$ films in an oxygen atmosphere. Consequently, the annealing in an oxygen atmosphere significantly reduced the surface roughness of the films (from 63 to 47 nm) and the density of droplets on the $LiNbO_3$ film surface. Annealing for 1 hour in an oxygen atmosphere under a temperature of 600 °C increases oxygen content in the film from 4.03 atm [38]. In the same year, Aleksei Sosunov et al., studied the effect of pre-annealing of $LiNbO_3$ in a specific range of temperature. Pre-annealing leads to an improvement in the structure of the subsurface layer of $LiNbO_3$, and a slight decrease in the refractive index caused by an increase in the homogeneity and a lower concentration of protons inside the crystal [39]. This work shows the preparation of $LiNbO_3$ films, and utilizing a single-step deposition process using the chemical bath deposition method without any post-heat treatment, the results were compared with the characteristics of another sample after heat treatment (slandered method) and the structural, morphological and optical properties have been investigated.

Experimental methods

Figure (1-a) shows the flow chart of the $LiNbO_3$ film preparation process using the chemical bath deposition process. The citric acid (CA) and ultra-pure (99.99%) niobium pentoxide without further purification have been used in the process. The solution has been prepared by combining Ethylene Glycol and citric acid in a glass beaker for 2 h, then mixing with continued stirring with Li_2Co_3 and Nb_2O_5 for 9 h at 90 °C. The following material weight was used Li_2Co_3 = 3.7 g, Nb_2O_5 = 13.30 g, CA = 10.5 g and EG = 20 g, respectively. According to previously published articles, the molar ratio between Nb_2O_5 and Li_2Co_3 was 1:1 [40]. After 12 h, two samples were prepared by inserting quartz substrates in the chemical bath for 30 minutes. Figure (1-a) gives the experimental work flowchart for comparison, one of the prepared samples was annealed in static air at 500 °C for 2 h while the second sample remains as it is. Figure (1-b) shows the quartz substrate vertically inserted in the solution baker. Optical interference was used to measure the thicknesses of the two samples. The structural properties of $LiNbO_3$ were analysed by using XRD (Shimadzu 6000). The surface morphology of $LiNbO_3$ was studied by (SEM) Scanning Electron Microscopy (InspectTM F50). The optical properties were studied using the double-beam ultraviolet-visible (UV-Vis).

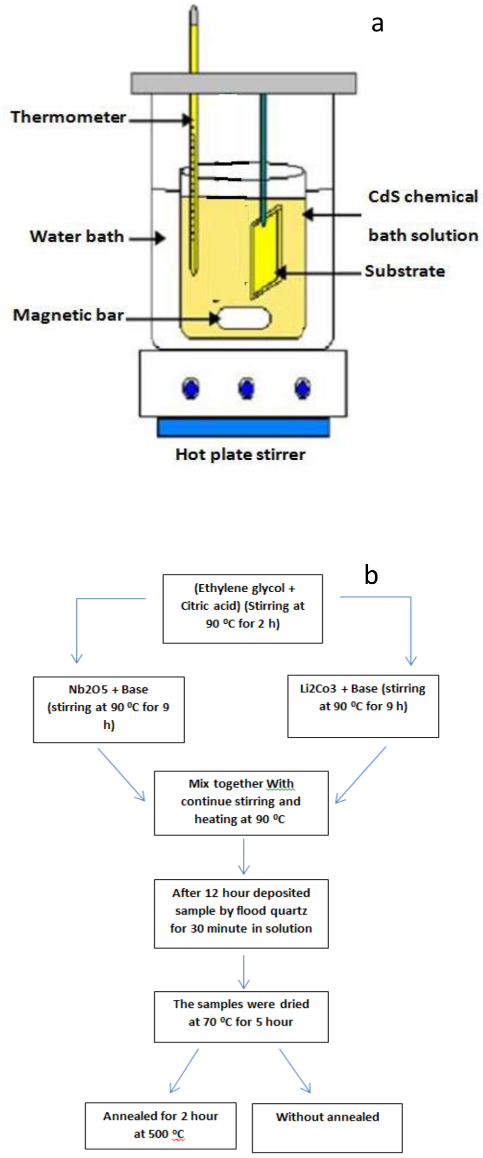

Fig.1 a-flowchart of $LiNbO_3$ nanostructure preparation process b-CBD technique

Results and discussion

Figure 2 shows the XRD of $LiNbO_3$ nanophotonics that was prepared by depositing on quartz substrates grown by the chemical bath deposition method. Figure. 2-a represents the XRD peaks of $LiNbO_3$ nanostructures beyond the annealing process, they were as follows: 2θ = 23.74, 32.71, 34.82, 47.61, 54.60 and 58.25 which belong to (012), (104), (110), (024), (116) and (122) diffraction planes, respectively. While the XRD peaks are at 2θ = 23.86, 32.44, 35.43, 48.14, 54.99, 58.20 which belong to (012), (104), (110), (024), (116) and (122), respectively, diffraction planes are related to sample without any post-heat treatment, all peaks belong to $LiNbO_3$ nanostructures and agree with other published works [41–44]. All the peaks could be indexed to the hexagonal structure with lattice parameters a = b = 5.1566, c = 13.858 according to the reference database coded [JCPDS (card no. 01-074-2239)]

A maximum diffraction peak was found at 2θ = 23.75 for annealed samples with a slight shifting toward 2θ = 23.86 for the sample without annealing caused by the strain and stress and dislocation that have been presented as shown in Table 1. The measured structural properties of $LiNbO_3$ are listed in Table 1. Crystallite size (D) was determined by utilizing Scherrer's formula [45].

Where K is a constant taken to be 0.94, λ is the wavelength X-ray used (λ = 1.54 Å), β is the full width at half maximum of the XRD pattern and θ is Bragg's angle. In addition, the strain (ε) and dislocation density (δ) of $LiNbO_3$ nanophotonics were calculated using the following relations [46].

$D = k\,\lambda/\beta \cos\theta$ (1)

$\delta = 1/D^2$ (2)

$\varepsilon = \beta/4 \tan\theta$ (3)

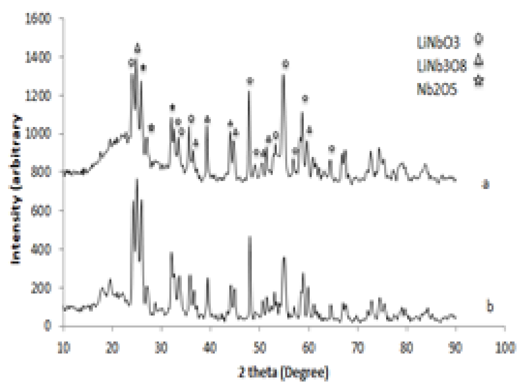

Fig. 2. XRD patterns of $LiNbO_3$ nanostructure a) with annealing , b) without annealing

Bragg's formula was used to determine the interplanar distance (d) for all sets of $LiNbO_3$ [46].

$d = n/2 \sin\theta$ (4)

In the obtained films that have polycrystalline-like nature, two phases could be identified which are the $LiNbO_3$ and $LiNb_3O_8$ phases. The preferred phase was found to be the $LiNbO_3$ phase that appeared at the 012 diffraction plane. The diffraction pattern shows the existence of a small amount of secondary Lithium (Li) deficient phase ($LiNb_3O_8$). This phase is originated in the two samples from an interface reaction between the oxygen and $LiNbO_3$ in the sample with annealing, it could be detected by XRD peaks of LiNb3O8 at 2θ = 24.45, 38.50 and 43.63 match with (400), (-403) and (420) planes, respectively [JCPDS (card no. 01-074-2239)]. The XRD peaks also detected this phase in the samples without annealing, these peaks were 2θ = 24.44, 38.58, 43.64 matches with (400), (-403) and (420) planes, respectively [JCPDS (card no. 01-074-2239)]. We note that there are different peaks at 2θ = 25.4 corresponding to (-212) planes [JCPDS (card no. 01-074-2239)]. Notably, the intensity of the peaks related to $LiNbO_3$ for the sample without annealing is higher than that of the annealed sample as shown in figure 2. However, this is associated with higher diffraction intensity for both $LiNb_3O_8$ phase and Nb_2O_3 material, thus, affecting the values of the energy gap. Other characteristics will be discussed later. The measured lattice constants showed good agreement with experimental values given in Table 2.

The optical absorbance spectra of the prepared LiNbO3 thin film with two samples, one of them has submitted to annealing via chemical bath deposition method while the other has not, as shown in figure 3 (a and b), respectively. From the absorption spectra in the figure, the peak position of absorption for both samples appears in the UV region. For the annealed sample, the absorption edge was (320–400 nm), whereas for the unannealed sample, the absorption edge was (310–400nm).

.

Table 1. Properties of the chemicals used in this work.

Names	Niobium pentoxide	Lithium carbonate	Citric acid	Ethylene glycol
Chemical formula	Nb_2O_5	Li_2Co_3	$C_6H_8O_7$	$C_2H_6O_2$
Supplier source	Aldrich	Montedison	Alfa Chemical	Alfa Chemical
Purity	99.99 %	99.99 %	99.99 %	99.99 %
Molar mass	265.81 g/mol	73.89 g/mol	192.123 g/mol (anhydrous), 210.14 g/mol (monohydrate)	62.068 g/mol
Appearance	White orthogonal solid	Odorless white powder	Odorless White solid	Odorless colorless liquid
Density	4.60 g/cm^3	2.11 g/cm^3	1.665 g/cm3 (anhydrous), 1.542 g/cm3	1.1132 g/cm^3 (0.04022 lb/cu in)
Melting point	1,512 ^{0}C(2,754 ^{0}F; 1,785 K)	723 ^{0}C(1,333 ^{0}F; 996 K)	156 ^{0}C (313 ^{0}F; 429 K)	-12.9 ^{0}C (8.8 ^{0}F; 260.2 K)

Table 2. $LiNbO_3$ nanophotonic parameters with annealing and without using XRD data

sample	Orientation hkl	Peak (2 theta)	Particle size (nm)	Dislocation Density (δ) (10 $^{-9}$) (lines/m $^{-2}$)	Strain (10 $^{-3}$)	dhkl	Lattice Constants a and c (A)
With annealing	012	23.75	8.042	1.54621E+12	0.430	3.75	a = 5.1566 c = 13.85
	104	32.60	4.093	5.96802E+12	0.814	2.74	a = 5.1566 c = 13.85
	110	35.22	6.475	2.38452E+12	0.506	2.55	a = 5.1566 c = 13.85
	024	48.63	8.406	1.41501E+12	0.357	1.88	a = 5.1566 c = 13.85
	116	54.74	6.955	2.06684E+12	0.410	1.69	a = 5.1566 c = 13.85
	122	58.25	12.702	6.19785E+11	0.217	1.64	a = 5.1566 c = 13.85
Without annealing	012	23.86	10.157	9.69273E+11	0.341	3.75	a = 5.1566 c = 13.85
	104	32.44	13.280	5.66995E+11	0.251	2.74	a = 5.1566 c = 13.85
	110	35.43	13.321	5.63508E+11	0.246	2.55	a = 5.1566 c = 13.85
	024	48.14	15.667	4.07374E+11	0.192	1.88	a = 5.1566 c = 13.85
	116	54.99	12.901	6.00787E+11	0.220	1.69	a = 5.1566 c = 13.85
	122	58.40	12.145	6.77906E+11	0.226	1.64	a = 5.1566 c = 13.85

In addition, as the wavelength decreases, the absorption increases. The absorption in the wavelength range of less than 400 nm indicates the transition of the electron from the upper part of the valence band to the lowest part of the conduction band. The UV-V is an absorption spectrum that exhibited a considerable wide 'shoulder' at about 405 nm (Figure 3). In the near UV range, owing to d-sp (inert-band) and sp-sp (intra-band) electronic transitions. An energy gap was obtained by plotting the graphic relationship between (a hn)^2 & hn (eV) plot. The obtained energy gap value is shown in figure 3. The value of the annealed sample was found to be about 3.65 ev while that of the unannealed sample is 3.64 ev. The results indicated that the unannealed sample band energy gap was equal to that of the annealed sample. The calculated values of the dielectric constant ($\varepsilon\infty$) were obtained using the $\varepsilon\infty$ = n2 relation found elsewhere [47]. Figure (4-a) shows the dielectric constant as a function of photon energy for the unannealed sample and an increase in optical dielectric constant with a decrease in photon energy. The extinction coefficient (k) plot as a function of photon energy shows that the extinction coefficient is decreased with an increase in photon energy, it is inversely associated with the absorbance spectra. Therefore, the low absorbance gives a high extinction coefficient which is similarly observed by Zhang et al., (2014) (Figure 4-a). Figure (4-b) shows the annealed sample. The dramatic change and increase in the value of e and Kex are caused by the complete formation of $LiNbO_3$ material after heat treatment which agrees with XRD results that show the moderate phase compared with the Nb_2O_5 phase.

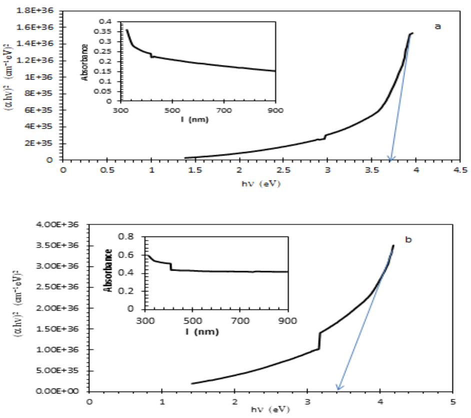

Figure. 3: LiNbO3 nanophotonics a) with annealing , b) without annealing

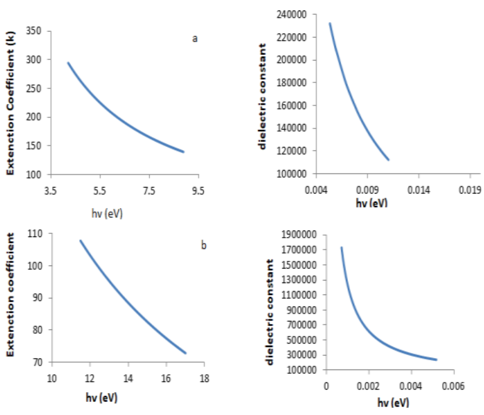

Figure 4. Extinction coefficient and dielectric constant at a) without annealing, b) with annealing

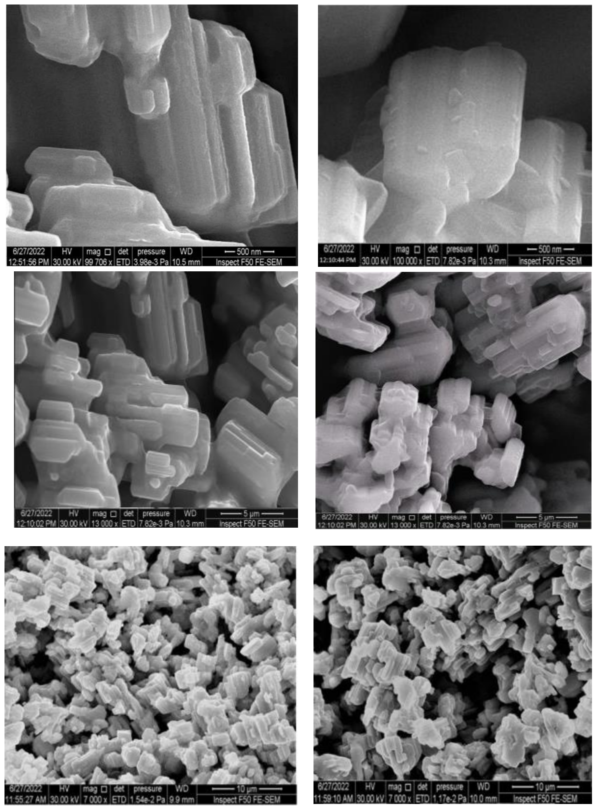

Figure.5 $LiNbO_3$ surface morphology a) after annealing process b) without annealing process .

The SEM microscope was used to test the surface morphology of the prepared films and presented in figure 5 (a and b). There are no essential differences found in the morphology of the two samples as observed in the figure, and they are both homogeneous and free from defects and dislocation. These ensure the clear similarity in both $LiNbO_3$ samples prepared with and without post-heat treatment.

A TEM Image of the prepared solution before deposited was obtained which may give an indication about the grain size of the prepared material before deposition using chemical bath deposition. The results show a particle size of about 500 nm and below. This agree with obtained with the results obtained from SEM Image where a clear increment and growth of the particle size after deposition process for a specific time.

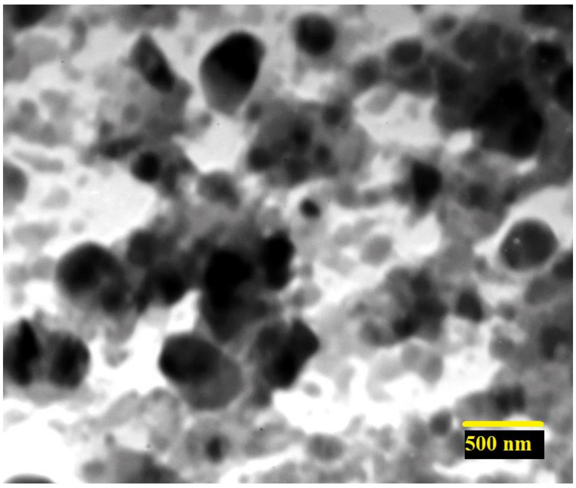

Figure 6.FTIR spectrum of $LiNbO_3$ single crystal grown by a Chemical bath deposition method, a) with annealing, b) without annealing.

The compositional profile of chemical bath deposition grown in $LiNbO_3$ is shown in Figure 7 along with the growth direction and diameter. Results show that in $LiNbO_3$, grown crystals were homogeneous in composition. In addition, the band at 560 cm^{-1} is related to the specific vibration of Li-O bonds. Moreover, the band 860 cm^{-1} is related to Nb-O-Nb stretching vibration. From the results, we noticed that the bonds between the materials are formed; the intensity of vibration of O-H bonds was stronger in the unannealed sample and the intensity of the phase of vibration of Nb-O-Nb was weaker. The intensity of vibration of O-H bonds is stronger in the non-annealing sample because as coal rank increased, the cyclic OH hydrogen bond decreased.it has been found that when heat treatment is done, the sample contains a percentage of carbon caused by the heat treatment. It is predicted that when coal rank increases (with annealing), the hydroxyl content will decrease similar behaviour could be found in other published work[48]. It is also widely known that the O-H bond caused significant problems with high leakage current and breakdown voltage. Therefore, after the film is deposited, O-H bonds must be weakened by higher temperature annealing above 350 °C [49].

Conflict of interest

The authors have declared no conflict of interest.

Acknowledgment

The authors would like to thank the department of applied science-university of Technology –Iraq for the logistic support of this work

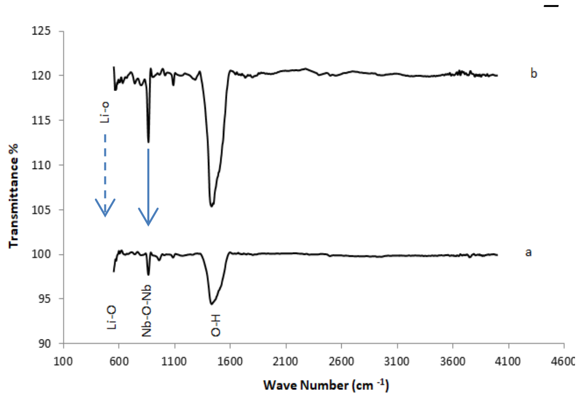

Figure 7.FTIR spectrum of $LiNbO_3$ single crystal grown by a Chemical bath deposition method, a) with annealing, b) without annealing.

Conclusion

From the obtained results it could be concluded that $LiNbO_3$ with dielectric properties and enhanced optical band gap could be successfully obtained on a quartz substrate via the chemical bath deposition method, with no post-heat treatment. The XRD results found that the prepared LiNbO3 has a polycrystalline-like structure caused by having various peaks in varying plane orientations. The morphology of the two samples is the same and they are both homogeneous and free from defects, as indicated in the SEM result. The UV-vis results indicated that the lower absorbance for the annealed sample with energy gap shifted from 3.54 to 3.65 after the annealing process. Therefore, the results from this work present the successful preparation of LiNbO3 dielectric material without any post-heat treatment. The obtained results ensure a good quality material with physical properties very close to the standard LiNbO3 material. The simplicity of the process and high yields make it possible and effective for industrial applications. As predicted, this simple chemical bath deposition method could be further extended to prepare another important multi-component oxide.

References

1. D. Janner, D. Tulli, M. Jofre, D. Yudistira, S. Balsamo, M. Belmonte, V. Pruneri, Domain inverted acousto- and electrooptic devices and their application to optical communication, sensing, laser sources, and quantum key distribution. IEEE J. Sel. Top. Quantum Electron. 19, 34006–34016 (2013)
2. Makram A Fakhri, Y Al-Douri, U Hashim, Evan T Salim, Solar Energy, 120: 381-388, (2015).

3. P. Kumar, S.M. Baru, S. Perero, R.M.L. Sai, I. Bhamik, S. Ganesamoorthy, A.K. Karnal, X-ray photoelectron spectroscopy, high-resolution X-ray direction and refractive index analyses of Ti-doped lithium niobate (Ti:LiNbO3) nonlinear optical single crystal. J. Phys. 75, 1035–1040 (2010)
4. Vakulov, Zakhar, Evgeny Zamburg, Daniil Khakhulin, Andrey Geldash, Dmitriy A. Golosov, Sergey M. Zavadski, Andrey V. Miakonkikh et al. "Oxygen pressure influence on properties of nanocrystalline LiNbO3 films grown by laser ablation." *Nanomaterials* 10, no. 7 (2020): 1371.
5. Barik, R., Satpathy, S. K., Behera, B., Biswal, S. K., & Mohapatra, R. K. (2020). Synthesis and Spectral Characterizations of Nano-Sized Lithium Niobate (LiNbO3) Ceramic. *Micro and Nanosystems*, *12*(2), 81-86.
6. Cena, C. R., Torsoni, G. B., & Freitas, G. Q. D. (2016). Synthesis of LiNbO 3 thin films by using niobium oxalate. *Matéria (Rio de Janeiro)*, *21*, 623-631.
7. B. Knabe, D. Schutze, T. Jungk, M. Svete, W. Assenmacher, W. Mader, K. Buse, Synthesis and characterization of Fe-doped LiNbO3 nanocrystals from a triple-alkoxide method. Phys. Status Solidi (A) 208, 857–862 (2011)
8. Tulli, Domenico. "Micro-nano structured electro-optic devices in LiNbO3 for communication and sensing." (2012).
9. J. Zhang, X. Zhang, Biomolecular binding dynamics in sensors based on metallic photonic crystals. Opt. Commun. 320, 56–59 (2014)
10. H. Lu, B. Sadani, G. Ulliac, N. Courjal, C. Guyot, J.-M. Merolla, M. Collet, F.I. Baida, M.-P. Bernal, 6-Micron interaction length ctro-optic modulation based on lithium niobate photonic crystal cavity. Opt. Express 20, 20884–20893 (2012)
11. H. Chen, T. Lv, A. Zheng, Y. Han, Discrete diffraction based on electro-optic effect in periodically poled lithium niobate. Opt. Commun. 294, 202–207 (2013)
12. P. Ganguly, Semi-analytical analysis of lithium niobate photonic wires. Opt. Commun. 285, 4347–4352 (2012)
13. A.A. Mohamed, M.A. Metawe'e, A.N.Z. Rashed, A.I.M. Bendary, Ultra high speed semiconductor electrooptic modulator devices for gigahertz operation in optical communication systems. Int. J. Opt. Appl. 1, 1–7 (2011)
14. K.S. Kaur, A.Z. Subramanian, Y.J. Ying, D.P. Banks, M. Feinaeugle, P. Horak, V. Apostolopoulos, C.L. Sones, S. Mailis, R.W. Eason, Waveguide mode filters fabricated using laserinduced forward transfer. Opt. Express 19, 9814–9819 (2011).
15. Grange, R.; Choi, J.W.; Hsieh, C.L.; Pu, Y.; Magrez, A.; Smajda, R.; Forro, L.; Psaltis, D. (2009). "Lithium niobate nanowires: synthesis, optical properties and manipulation". Applied Physics Letters. 95 (14): 143105. Bibcode:2009ApPhL..95n3105G. doi:10.1063/1.3236777. Archived from the original on 2016-05-14.
16. Grigas, A; Kaskel, S (2011). "Synthesis of LiNbO3 nanoparticles in a mesoporous matrix". Beilstein Journal of Nanotechnology. 2: 28–33. doi:10.3762/bjnano.2.3. PMC 3045940. PMID 21977412.
17. Gong, S., Song, Y. H., Manzaneque, T., Lu, R., Yang, Y., & Kourani, A. (2017, August). Lithium niobate MEMS devices and subsystems for radio frequency signal processing. In 2017 IEEE 60th International Midwest Symposium on Circuits and Systems (MWSCAS) (pp. 45-48). IEEE.
18. Qi, Y., & Li, Y. (2020). Integrated lithium niobate photonics. Nanophotonics, 9(6), 1287-1320.
19. W. Branch, et al., Investigation of a solid-state tuning behavior in lithium niobate, IEEE Trans. Ultrason. Ferroelectrics Freq. Contr. 67 (2) (2020) 365–373.
20. J. Dai, R. Xu, Y.S. Lin, C.H. Chen, Tunable electromagnetic characteristics of suspended nanodisk metasurface, Optic Laser. Technol. 128 (2020).
21. P.K. Anand Prem, A. Chakrapani, "A millimeter-wave generation scheme based on frequency octupling using LiNbO3 mach–zehnder modulator, Natl. Acad. Sci. Lett. 42 (5) (2019).
22. B.S. Tang, C.X. Sun, Adjustment for mid-infrared narrow-band filtering characteristics in multilayer graphene nanofilms, Guangxue Jingmi Gongcheng/ Optics Precis. Eng. 27 (12) (2019).
23. P.J. Turner, et al., 5 GHz band n79 wideband microacoustic filter using thin lithium niobate membrane, Electron. Lett. 55 (17) (2019).
24.] M. Bazzan, C. Sada, M. Bazzan, C. Sada, Optical waveguides in lithium niobate : recent developments and applications Optical waveguides in lithium niobate : recent developments and applications, Appl. Phys. Rev. 2 (4) (2015), 040603, 040603–1.
25. I. Bolesta, M. Vakiv, V. Haiduchok, O. Kushnir, R. Gamernyk, Optical properties of LiNbO 3 -Ag nanocomposites, International Conference on Oxide Materials for Electronic Engineering 133 (4) (2018) 860–863.
26. Makram, A. F., Alwazni, M. S., Yarub, A. D., Salim, E. T., Uda, H., & Woei, C. C. (2016). Preparation of nanophotonics LiNbO3 thin films and studying their morphological and structural properties by sol-gel method for waveguide applications. *International Journal of Chemical and Molecular Engineering*, *10*(5), 519-524.
27. Garibay-Alvarado, J. A., Farías, R., & Reyes-López, S. Y. (2019). Sol-gel and electrospinning synthesis of lithium niobate-silica nanofibers. *Coatings*, *9*(3), 212.
28. M. Liu, D. Xue, K. Li, Soft-chemistry synthesis of LiNbO3 crystallites. J. Alloy. Compd. 449, 28–31 (2013)
29. X. Wang, Y. Liang, S. Tian, W. Man, J. Jia, Oxygen pressure dependent growth of pulsed laser deposited LiNbO3 films on diamond for surface acoustic wave device application. J. Cryst. Growth 375, 73–77 (2013)
30. Meriche, F., Boudrioua, A., Kremer, R., Dogheche, E., Neiss-Clauss, E., Mouras, R., ... & Boutaoui, N. (2010). Fabrication and investigation of 1D and 2D structures in LiNbO3

thin films by pulsed laser ablation. *Optical Materials*, *32*(11), 1427-1434.
31. Tanaka, A., Miyashita, K., Tashiro, T., Kimura, M., & Sukegawa, T. (1995). Preparation of lithium niobate films by metalorganic chemical vapor deposition with a lithium alkoxide source. Journal of crystal growth, 148(3), 324-326.
32. Callejo, D., Bermudez, V., Serrano, M. D., & Diéguez, E. (2002). Lithium niobate films on periodic poled lithium niobate substrates prepared by liquid phase epitaxy. Journal of crystal growth, 237, 596-601.
33. Iyevlev, V., Kostyuchenko, A., Sumets, M., & Vakhtel, V. (2011). Electrical and structural properties of LiNbO3 films, grown by RF magnetron sputtering. Journal of Materials Science: Materials in Electronics, 22(9), 1258-1263.
34. Deon, V. G., Thesing, A., Santana, L. R., Costa, V. C., Vaz, M. O., Silva, R. M., ... & Carreno, N. L. (2021). Synthesis of LiNbO3 nanocrystals by microwave-assisted hydrothermal method: formation mechanism and application to hydrogen evolution reaction. *Chemical Papers*, *75*(8), 3807-3815.
35. Deon, V. G., Thesing, A., Santana, L. R., Costa, V. C., Vaz, M. O., Silva, R. M., ... & Carreno, N. L. (2021). Synthesis of LiNbO3 nanocrystals by microwave-assisted hydrothermal method: formation mechanism and application to hydrogen evolution reaction. Chemical Papers, 75(8), 3807-3815.
36. Kiselev, D. A., et al. "Effect of annealing on the structure and phase composition of thin electro-optical lithium niobate films." Inorganic Materials 50.4 (2014): 419-422.
37. Fakhri, Makram A., et al. "Annealing temperature effect on structural and morphological properties of nano photonic LiNbO3." Journal of Materials Science: Materials in Electronics 28.22 (2017): 16728-16735.
38. Klimin, Viktor S., et al. "Influence of annealing on nanocrystalline LiNbO3 films properties." International Conference on Micro-and Nano-Electronics 2018. Vol. 11022. SPIE, 2019.
39. Sosunov, Aleksei, Roman Ponomarev, Oksana Semenova, Igor Petukhov, and Anatoly Volyntsev. "Effect of pre-annealing of lithium niobate on the structure and optical characteristics of proton-exchanged waveguides." Optical Materials 88 (2019): 176-180.
40. Fakhri, Makram A., et al. "Optical investigation of nanophotonic lithium niobate-based optical waveguide." Applied Physics B 121.1 (2015): 107-116.
41. Fakhri, Makram A., Y. Al-Douri, Uda Hashim, and Evan T. Salim. "XRD analysis and morphological studies of spin coated LiNbO3 nano photonic crystal prepared for optical waveguide application." In Advanced Materials Research, vol. 1133, pp. 457-461. Trans Tech Publications Ltd, 2016.
42. Fakhri, Makram A., et al. "XRD analysis and morphological studies of spin coated LiNbO3 nano photonic crystal prepared for optical waveguide application." Advanced Materials Research. Vol. 1133. Trans Tech Publications Ltd, 2016.
43. Fakhri, M. A., Salim, E. T., Hashim, U., Salim, Z. T., & Minshed, M. A. (2017). Effects of different parameters on XRD properties of nano and micro LiNbO3 using chemical method. Adv Nano Energy, 1(2), 98-106.
44. Y. Al-Douri, Q. Khasawneh, S. Kiwan, U. Hashim, S.B. Abd Hamid, A.H. Reshak, A. Bouhemadou, M. Ameri, R. Khenata, Structural and optical insights to enhance solar cell performance of CdS nanostructures. Energy Convers. Manag. 82, 238–243 (2014).
45. Y. Al-Douri, Q. Khasawneh, S. Kiwan, U. Hashim, S.B. Abd Hamid, A.H. Reshak, A. Bouhemadou, M. Ameri, R. Khenata, Structural and optical insights to enhance solar cell performance of CdS nanostructures. Energy Convers. Manag. 82, 238–243 (2014)
46. J. Zhang, X. Zhang, Biomolecular binding dynamics in sensors based on metallic photonic crystals. Opt. Commun. 320, 56–59 (2014).
47. Chen, J., Liu, L., Liu, H., Li, Y., Wang, J., Mu, X., ... & Zhang, X. D. (2020). Ultrabright bimetallic AuAg complex: From luminescence mechanism to biological application. Journal of Innovative Optical Health Sciences, 13(05), 2041001.
48. Li, R., Tang, Y., Che, Q., Ma, P., Luo, P., Lu, X., & Dong, M. (2022). Effects of Coal Rank and Macerals on the Structure Characteristics of Coal-Based Graphene Materials from Anthracite in Qinshui Coalfield. *Minerals*, *12*(5), 588.
49. Horita, S. (2019). Highly effective removal of OH bonds in low-temperature silicon oxide films by annealing with ammonia gas at a low temperature of 175° C. Japanese Journal of Applied Physics, 58(3), 038002.